JPE 16-2-19

http://dx.doi.org/10.6113/JPE.2016.16.2.584
ISSN(Print): 1598-2092 / ISSN(Online): 2093-4718

Transient Performance Improvement in the Boundary Control of Boost Converters using Synthetic Optimized Trajectory

Gaohui Feng†, Liqiang Yuan*, Zhengming Zhao*, Junjie Ge**, Xiuxi Ye*, and Ting Lu*

†,*State Key Laboratory of Power System, Dept. of Electrical Engineering, Tsinghua University, Beijing, China
**Corporate Research, ABB (China) Ltd., Beijing, China

Abstract

This paper focuses on an improvement in the transient performance of Boost converters when the load changes abruptly. This is achieved on the basis of the nature trajectory in Boost converters. Three key aspects of the transient performance are analyzed including the storage energy change law in the inductors and capacitors of converters during the transient process, the ideal minimum voltage deviation in the transient process, and the minimum voltage deviation control trajectory. The changing relationship curve between the voltage deviation and the recovery time is depicted through analysis and simulations when the load suddenly increases. In addition, the relationship curve between the current fluctuation and the recovery time is obtained when the load suddenly decreases. Considering the aspects of an increasing and decreasing load, this paper proposes the transient performance synthetic optimized trajectory and control laws. Through simulation and experimental results, the transient performances are compared with the other typical three control methods, and the ability of proposed synthetic trajectory and control law to achieve optimal transient performance is verified.

Key words: Boost converters, Boundary control, Recovery time, Synthetic trajectory, Voltage deviation

I. INTRODUCTION

DC-DC converters, including Buck, Boost, Buck-Boost, and Cuk converters are high non-linear systems [1, 2]. The analysis methods are presently in use are the Average Model Method (AMM) [3] and the Geometric Graphic Method (GGM) [4]. The average model method combines the responses of several different topologies in a control period with a small-signal assumption, takes the nonlinear time-varying circuit as a linear time-invariant circuit, and uses the linear method for analysis. This method demands that the switching frequency of the converters be much greater than the circuit characteristic frequency. It also demands that the circuit inputs are constant or slowly varying values. In comparison, the geometric graphic method does not make a small-signal assumption and keeps the nonlinear feature. It uses a phase plane to show the dynamic process, and determines the converters' inherent dynamic and static characteristics in accordance with their geometrical properties. Compared with the AMM, it is more suitable for the analysis of suddenly changing loads. Actually, the AMM is a kind of frequency domain method while the GGM is a kind of time domain method.

The PI control method is typically a kind of AMM and there are many others methods used in DC-DC converters. The passivity-based control used in high-power Buck converters ensures dynamic and steady-state responses [5]. A simplified parallel-damped passivity-based controller combined with a PID controller can obtain better performance from Boost converters [6]. Compared with the conventional sliding mode control (SMC), other variants of the SMC have been proposed to improve the performance of DC-DC converters [7]-[10]. One-cycle control is applicable to large-signal nonlinear systems, and the improved one-cycle control can reject both the source side and load side disturbances of DC-DC converters [11], [12]. Synergetic control is used in DC-DC converters to

Manuscript received Jun. 20, 2015; accepted Sep. 24, 2015
Recommended for publication by Associate Editor Se-Kyo Chung.
†Corresponding Author: fgh1980fgh@163.com
Tel: +86-10-6277-3237, Fax: +86-10-6279-4915, Tsinghua University
*State Key Laboratory of Power System, Dept. of Electrical Engineering, Tsinghua University, China
**Corporate Research, ABB(China)Ltd, China

achieve better dynamic performance and a faster response [13], [14]. Energy-based control uses the measured or estimated energy in the inductors and capacitors of converters to construct the control structures [15], [16].

Boundary control is typically a kind of GGM [17]. When combined with the phase plane, it is widely used in Buck converters [18], [19], Boost converters [20], [34], single-phase inverters [21], [22], three-phase PWM inverters [23], single-phase power factor correctors (PFCs) [24], [25] and dual-active-bridge (DAB) converters [26]. The trajectory used in boundary control is called the switching surface (SS). The SS has a first-order SS, a second-order SS, a high-order SS, and so on [27]-[29].

In a study of the different kinds of SSs in Buck converters, the natural trajectory was used as a SS for achieving excellent transient performance without an overshoot during startup [30]. The natural trajectory of Boost converters was deduced and an improved boundary control using the natural trajectory as an SS was shown to accomplish the dynamic process at the fastest speed without an overshoot [31]. A curved SS for a single inverter was studied and the improved boundary control enhanced its dynamic regulation performance both in light load and overload conditions [32]. A novel direct power control (DPC) using the natural SS of a three-phase PWM rectifier was proposed by combining the DPC with boundary control, which can greatly improve the dynamic performance of the DC output voltage [23]. Because the minimum output voltage deviation and the minimum recovery time cannot be obtained simultaneously, novel control laws using energy balancing were proposed to achieve a superior tradeoff between the voltage deviation and recovery time [33]. This novel control has better dynamic performance than the PI control and the synergetic control. Diagrams of the voltage deviation and the recovery time were given in the new control law. However, its analysis is limited to a situation where the load power suddenly increases the load power.

In this paper, a distinctive SS formed by several types of trajectories, namely the synthetic optimized trajectory, is introduced. After analyzing and utilizing the energy change law during the sudden load changes in Boost converters, the minimum voltage deviation trajectory and its control law are presented. The optimal SS is composed of several natural trajectories and its shape can be changed by using two parameters for acquiring suitable performance. Under this control law, the relationship between the voltage deviation and the recovery time is deduced and it is shown to be superior to the control method proposed in [33]. The relationship between the inductor current fluctuation and the recovery time in boost converters is also derived.

II. Minimum Recovery Time Controls

The topology of Boost converters, as shown in Fig. 1, is composed of passive circuit components, a load, energy storage elements (L_b and C_b), power semiconductor (S and D), and power sources (U_{in}). In Fig.1, U_{in} is the input voltage, i_{bL} is the inductor current, i_{bc} is the capacitor current, u_{bC} is the capacitor voltage or the output voltage u_O, and i_{bo} is the output current.

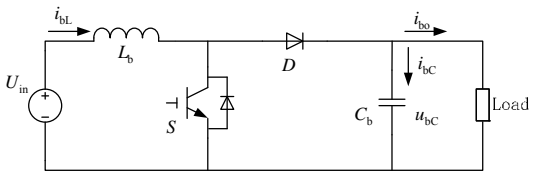

Fig. 1. Configuration of boost converters.

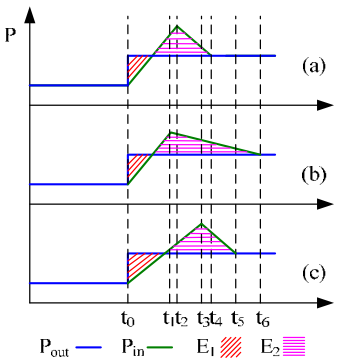

Fig. 2. Energy changes in different control methods.

A. Time optimization

Time optimization means reducing the recovery time in the dynamic process when a load suddenly changes. For example, when the load increases abruptly, the voltage fluctuates. The period of the voltage deviation is the recovery time. In the steady state, before and after the process, only the inductor current changes. This indicates that the whole energy change in the Boost converter is just the change of the inductor storage energy. The energy change of a Boost converter is shown in Fig. 2, which reveals that the excessive energy in the Boost converter is the integral of the power change between the input and output ports. It is a certain value under different control methods. E_1 is the input energy, and E_2 is the output energy. According to the energy balance, the change of the inductor energy is:

$$\Delta E_{bL} = E_2 - E_1 \tag{1}$$

Fig. 2(a) shows the energy change with the time-optimal control method. The switch is turned on at t_0 and turned off at t_2. The increased and decreased input power in the Boost converter is transferred at the fastest speed. As a result, its transient time is the shortest. Fig. 2(b) and Fig. 2(c) show the energy change with the conventional control method. The switch is turned off prematurely at t_1 in Fig. 2(b). The increased power is smaller than the power at t_2. Therefore, the transient time of Fig. 2(b) is longer than that of Fig. 2(a). If the switch is turned off late at t_3 in Fig. 2(c), the increased power is larger

than the power at t_2. Meanwhile, the power decreases at a limited speed. Therefore, the whole transient time of Fig. 2(c) exceeds that of Fig. 2(a).

In view of the above analysis, to obtain the shortest recovery time, the switch should be controlled to make the inductor current increase or decrease at the fastest speed, and the turning point of the switch should be obtained through the natural trajectory of the Boost converter.

B. Nature Trajectory

The unified transformations are defined as (2):

$$\begin{cases} U_{\text{inn}} = U_{\text{in}} \\ u_{\text{bCn}} = u_{\text{bC}} \\ u_{\text{bCn\_0}} = u_{\text{bC\_0}} \\ i_{\text{bOn}} = \sqrt{\dfrac{L_{\text{b}}}{C_{\text{b}}}} i_{\text{bO}} \\ i_{\text{bLn}} = \sqrt{\dfrac{L_{\text{b}}}{C_{\text{b}}}} i_{\text{bL}} \\ i_{\text{bLn\_0}} = \sqrt{\dfrac{L_{\text{b}}}{C_{\text{b}}}} i_{\text{bL\_0}} \end{cases} \tag{2}$$

The off-state natural trajectory of the Boost converter can be expressed as:

$$\left(U_{\text{inn}} - u_{\text{bCn}}\right)^2 + \left(i_{\text{bOn}} - i_{\text{bLn}}\right)^2 = h^2 \tag{3}$$

where h varies with the initial circuit state, which is expressed as:

$$\left(U_{\text{inn}} - u_{\text{bCn\_0}}\right)^2 + \left(i_{\text{bOn}} - i_{\text{bLn\_0}}\right)^2 = h^2 \tag{4}$$

The on-state nature trajectory of the Boost converter can be expressed as:

$$i_{\text{bLn}} = -\frac{U_{\text{inn}}}{i_{\text{bOn}}} u_{\text{bCn}} + l \tag{5}$$

where l varies with the initial circuit state, which is expressed as:

$$l = i_{\text{bLn\_0}} + \frac{U_{\text{inn}}}{i_{\text{bOn}}} u_{\text{bCn\_0}} \tag{6}$$

$u_{\text{bC\_0}}$ and $i_{\text{bl\_0}}$ are the circuit initial values. As shown in Fig. 3, the off-state natural trajectories in the unified phase plane are a family of circles, where the centers are the same point S(U_{inn} , i_{bOn}) and the radiuses are h. The on-state natural trajectory in the phase plane are a family of parallel straight lines. The intercept on the vertical axis is l in Fig. 3.

According to the balance of the output power and the input power in the steady state: $u_{\text{bCn}}i_{\text{bOn}}=U_{\text{inn}}i_{\text{bLn}}$, which can be described as:

$$i_{\text{bLn}} = \frac{i_{\text{bOn}}}{U_{\text{inn}}} u_{\text{bCn}} \tag{7}$$

This is called the load curve σ in Fig. 3. Assuming that the target operating point is T($u_{\text{bCn\_T}}$, $i_{\text{bln\_T}}$), point T is in the load curve. The circuit center and the origin of the coordinates are also in σ.

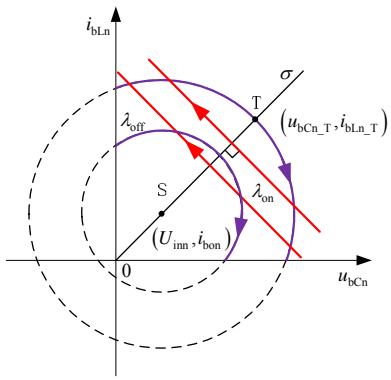

Fig. 3. On-state and off-state natural trajectory.

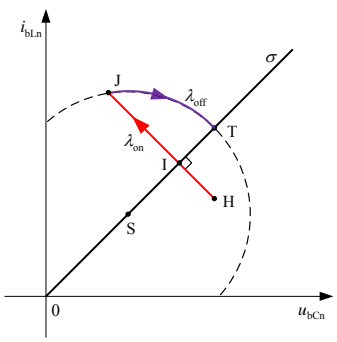

Fig. 4. The minimum recovery time trajectory.

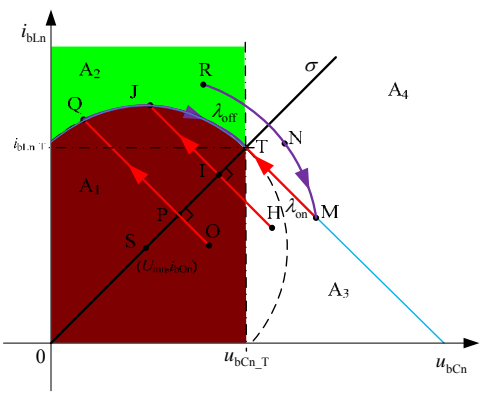

Fig. 5. The minimum recovery time control path.

C. The minimum time trajectory and control law

To get the shortest recovery time, the inductor current must vary at the fastest speed until the circuit goes back to the steady state. From the natural trajectory it is shown that the operation time in the on-state natural trajectory is proportional to the line length, and that the operation time in the off-state trajectory is proportional to the arc angle. Therefore, the shortest path is as shown in Fig. 4. Point H is the start operating point of the converter, and T is the target operating point after the change. The switch is on from Point H to Point J, and it is off from Point J to Point T. In this way, the dynamic process is the

fastest.

The time-optimal trajectory is shown in Fig. 5. The first quadrant is divided into four regions based on the off-state natural trajectory crossing the target point T, the on-state natural trajectory crossing T, and the vertical line crossing T. When selecting the on-state natural trajectory or the off-state natural trajectory as the SS, if the current voltage is below the target voltage, select the off-state natural trajectory as the SS, and if the voltage is higher than the target voltage, select the on-state natural trajectory as the SS. In Fig. 5, the operation paths, where the starting operation points are in different regions, are depicted and their control laws are presented as follows.

Case I : $u_{bCn}<u_{bCn\_T}$

if $\lambda_{off}<0$, then S=1, and the start operation point is in the A_1 region; otherwise S=0, and the point is in the A_2 region.

Case II: $u_{bCn}>u_{bCn\_T}$

If $\lambda_{on}<0$, then S=1, and the start operation point is in the A_3 region, otherwise S=0, and the point is in the A_4 region.

The equation S=0 means the switch is off, and the equation S=1 means the switch is on.

$$\lambda_{off}=\left(U_{inn}-u_{bCn}\right)^2+\left(i_{bLn}-i_{bOn}\right)^2 -\left(U_{inn}-u_{bCn\_T}\right)^2-\left(i_{bLn\_T}-i_{bOn}\right)^2 \tag{8}$$

$$\lambda_{on}=i_{bLn}+\frac{U_{inn}}{i_{bOn}}u_{bCn}-i_{bLn\_T}-\frac{U_{inn}}{i_{bOn}}u_{bCn\_T} \tag{9}$$

III. Minimum Voltage Deviation Controls

When the DC bus voltage deviation of the converter needs to be as small as possible, the minimum voltage deviation trajectory needs to be explored. In this section, in accordance with the direction of the storage energy change in the converters, the theoretical minimum voltage deviation is deduced and the control law of the trajectory of the minimum voltage deviation is proposed.

A. Storage Energy Circle of Boost Converters

The storage energy in a Boost converter is the sum of the inductor energy and the capacitor energy, which is:

$$E_{bLC}=\frac{1}{2}C_b{u_{bC}}^2+\frac{1}{2}L_b{i_{bL}}^2 \tag{10}$$

Under unified transformations (2), it can also be expressed as follows:

$${E_{bLCn}}={u_{bCn}}^2+{i_{bLn}}^2={r_b}^2 \tag{11}$$

Where:

$$E_{bLCn}=\frac{2E_{bLC}}{C_b} \tag{12}$$

As shown in Fig. 6, Equation (11) indicates a series of circles in the phase plane ∅, of which the center is the coordinate origin. The radius of the energy circle represents the storage energy in the converters. These circles are called the storage energy circles of the Boost converters.

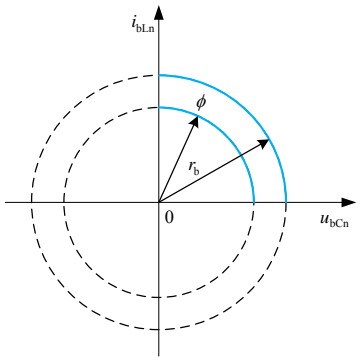

Fig. 6. Storage energy circle.

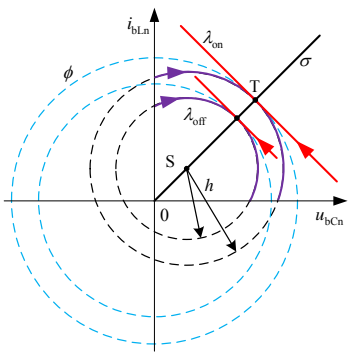

Fig. 7. The relationship between storage energy circle and nature trajectory.

The radius r_b of the storage energy circle is:

$$r_b=\sqrt{{u_{bCn}}^2+{i_{bLn}}^2}=\sqrt{E_{bLCn}} \tag{13}$$

The voltage and current in the same circle are different. However, the storage energy is the same.

From the previous conclusion, the tangent slope of each point in the off-state natural trajectory λ_{off} is:

$$s_{off}=\frac{di_{bLn}/dt}{du_{bCn}/dt}=\frac{U_{inn}-u_{bCn}}{i_{bLn}-i_{bOn}} \tag{14}$$

The tangent slope of the on-state natural trajectory λ_{on} is described as:

$$s_{on}=\frac{di_{bLn}}{du_{bCn}}=\frac{U_{inn}}{-i_{bOn}} \tag{15}$$

The slope of the load curve σ is:

$$s_{\sigma}=\frac{di_{bLn}}{du_{bCn}}=\frac{i_{bOn}}{U_{inn}} \tag{16}$$

Therefore, λ_{on} and σ are perpendicular.

$$s_{\sigma}s_{on}=-\frac{i_{bOn}}{U_{inn}}\frac{U_{inn}}{i_{bOn}}=-1 \tag{17}$$

The tangent slope of the storage energy circle ∅ is:

$$s_{bE}=\frac{di_{bLn}}{du_{bCn}}=-\frac{u_{bCn}}{i_{bLn}} \tag{18}$$

At the T point, the following formulas are established.

$$s_{on\_T}=-\frac{U_{inn}}{i_{bOn}}=-\frac{u_{bCn\_T}}{i_{bLn\_T}}=\frac{U_{inn}-u_{bCn\_T}}{i_{bLn\_T}-i_{bOn}}=s_{off\_T} \tag{19}$$

$$s_{\mathrm{bE\_T}} = -\frac{u_{\mathrm{bCn\_T}}}{i_{\mathrm{bLn\_T}}} = s_{\mathrm{on\_T}} = s_{\mathrm{off\_T}} = -\frac{1}{s_\sigma} \tag{20}$$

It is shown in Fig. 7 that the tangent slopes of the off-state natural trajectory and the on-state natural trajectory are equal, and that λ_{off} and σ are perpendicular at T. Meanwhile, ∅, λ_{on} and σ are tangent and ∅ is perpendicular to the load curve σ.

B. Energy Change Region

As shown in Fig. 8, when the operation point is at Point A under σ and the switch is on, the operation point will move to Point B ($u_{\mathrm{bCn\_B}}$,$i_{\mathrm{bLn\_B}}$) along λ_{on}. The radius of the energy circle r_B when Point B is on, is smaller than the radius of the energy circle r_A when Point A is on. This indicates that the energy in the circuit decreases. When the switch is off at Point B, the operation point will move to Point C along λ_{off}. The radius of the energy circle r_C when Point C is on, is smaller than r_B. This indicates that the energy in the circuit decreases as well.

As for the point under σ like Point B, there is:

$$i_{\mathrm{bLn\_B}} < \frac{i_{\mathrm{bOn}}}{U_{\mathrm{inn}}} u_{\mathrm{bCn\_B}} \tag{21}$$

It can be derived that:

$$s_{\mathrm{bE\_B}} = -\frac{u_{\mathrm{bCn\_B}}}{i_{\mathrm{bLn\_B}}} < -\frac{U_{\mathrm{inn}}}{i_{\mathrm{bOn}}} = s_{\mathrm{on\_B}} \tag{22}$$

$$s_{\mathrm{bE\_B}} = -\frac{u_{\mathrm{bCn\_B}}}{i_{\mathrm{bLn\_B}}} > \frac{U_{\mathrm{inn}} - u_{\mathrm{bCn\_B}}}{i_{\mathrm{bLn\_B}} - i_{\mathrm{bOn}}} = s_{\mathrm{off\_B}} \tag{23}$$

This indicates that the slope of ∅ is smaller than the slope of λ_{on} and larger than the slope of λ_{off} under σ. This implies that the radius of ∅ must decrease along the direction of λ_{on} or λ_{off}. The storage energy is certainly reduced along with the natural trajectory under σ.

Similarly, as shown in Fig. 9, when the operation point is at Point D above σ and the switch is on, the operation point will move to Point E ($u_{\mathrm{bCn\_E}}$,$i_{\mathrm{bLn\_E}}$) along λ_{on}. r_E is larger than r_D, which indicates that the energy in the circuit increases. When the switch is off at Point E, the operation point will move the Point F along λ_{off}. r_F is larger than r_E. Thus, the energy in the circuit increases as well.

As for the point under σ like E, there is:

$$i_{\mathrm{bLn\_E}} > \frac{i_{\mathrm{bOn}}}{U_{\mathrm{inn}}} u_{\mathrm{bCn\_E}} \tag{24}$$

It can be derived that:

$$s_{\mathrm{bE\_E}} = -\frac{u_{\mathrm{bCn\_E}}}{i_{\mathrm{bLn\_E}}} > -\frac{U_{\mathrm{inn}}}{i_{\mathrm{bOn}}} = s_{\mathrm{on\_E}} \tag{25}$$

$$s_{\mathrm{bE\_E}} = -\frac{u_{\mathrm{bCn\_E}}}{i_{\mathrm{bLn\_E}}} < \frac{U_{\mathrm{inn}} - u_{\mathrm{bCn\_E}}}{i_{\mathrm{bLn\_E}} - i_{\mathrm{bOn}}} = s_{\mathrm{off\_E}} \tag{26}$$

Therefore, the slope of ∅ is larger than that of λ_{on} and smaller than that of λ_{off} above σ. This implies that the radius of ∅ must be increasing along the directions of λ_{on} and λ_{off}. The storage energy is certainly increased along with the natural trajectory above σ.

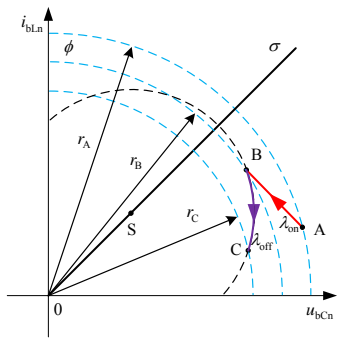

Fig. 8. Region of energy decreasing.

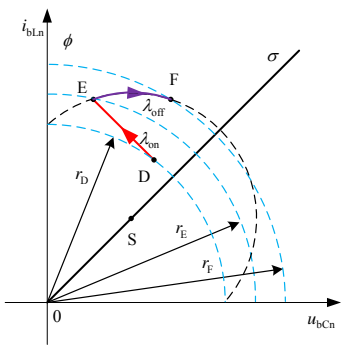

Fig. 9. Region of energy increasing.

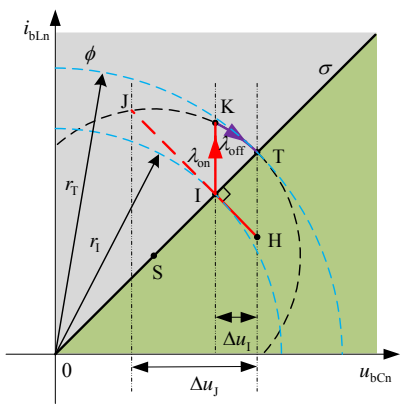

Fig. 10. Theoretical minimum voltage deviation trajectory.

C. Theoretical minimum voltage deviation

When the operation point is at Point H and the load suddenly increases, the trajectory of the shortest time along λ_{on} and λ_{off} is shown in Fig. 10. From Point H to Point T, the storage energy is increased. In accordance with the energy change law, the path must pass through σ and the intersection Point I ($u_{\mathrm{bCn\_I}}$,$i_{\mathrm{bLn\_I}}$) has the theoretical minimum voltage deviation Δu_I, which is much smaller than the whole voltage deviation Δu_J. To keep the minimum voltage deviation in the whole process, a possible operating path is shown in Fig. 10, which is the line segment HIKT. The line IK is composed of multiple segments of on-state and off-state natural trajectories.

According to (5) and (7), $u_{\mathrm{bCn\_I}}$ can be derived and the theoretical minimum voltage deviation $\Delta u_I = u_T - u_{\mathrm{bCn\_I}}$.

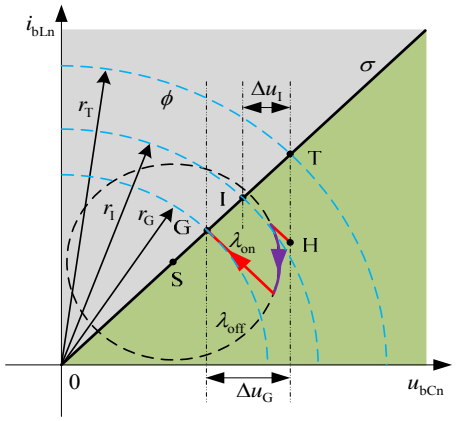

Fig. 11. Large voltage deviation trajectory.

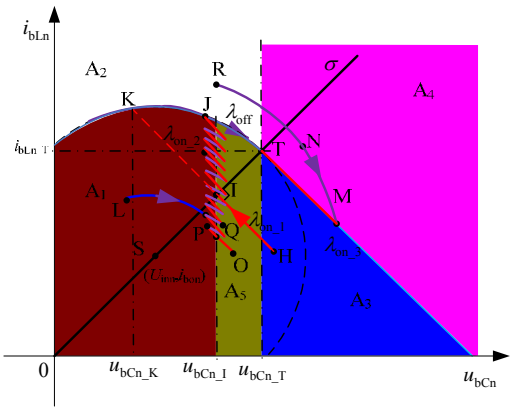

Fig. 12. The minimum voltage deviation control path.

As shown in Fig. 11, when the switch is off before reaching σ, the new cross Point G on σ will have a larger deviation Δu_G. This takes more time. Furthermore, the energy of Point G is smaller than that of Point I. As a result, more energy and time will be needed to reach Point T. Therefore, keeping the switch on until reaching Point I is the best choice.

D. The minimum voltage deviation trajectory and control law

The path of the minimum voltage deviation trajectory is shown in Fig. 12. Compared with the theoretical minimum voltage deviation in Fig. 10, the setting of the actual voltage value u_{bCn_I} should consider the sampling frequency and the control frequency of the voltage ripple. The higher the sampling and control frequency, the smaller the voltage ripple and the longer the recovery time, as in segment PJ in Fig. 12. Compared with the time-optimal trajectory, the A_1 region in Fig. 5 is divided into the A_5 region for executing the minimum voltage deviation. In this region, the operation path is along with the on-state natural trajectory. At the junction of these two regions, according to the hysteresis width, the path is composed of the on-state and off-state natural trajectories until it reaches Point J. The operation paths starting from the other regions are depicted and the control law are as follows.

Case I : $u_{bCn}<u_{bCn\_T}$

If $\lambda_{off}>0$, then S=0, and the start operation point is in the A_2 region. If $\lambda_{off}<0$ and $\lambda_{on\_2}<0$, then S=0, and the start operation point is in the A_1 region. If $\lambda_{off}<0$ and $\lambda_{on\_2}>0$, then S=1, and the start operation point is in the A_5 region.

Case II: $u_{bCn}>u_{bCn\_T}$

If $\lambda_{on\_3}>0$, then S=0, and then start operation point is in the A_4 region; otherwise S=1, and the start operation point is in the A_3 region.

The equation S=0 means the switch is off, and the equation S=1 means the switch is on.

$$\lambda_{off} = \left(U_{inn} - u_{bCn}\right)^2 + \left(i_{bLn} - i_{bOn}\right)^2 - \left(U_{inn} - u_{bCn\_T}\right)^2 - \left(i_{bLn\_T} - i_{bOn}\right)^2 \quad (27)$$

$$\lambda_{on\_1} = i_{bLn} + \frac{U_{inn}}{i_{bOn}} u_{bCn} - i_{bLn\_T} - \frac{U_{inn}}{i_{bOn}} u_{bCn\_T} \quad (28)$$

$$\lambda_{on\_2} = u_{bCn} - \left[u_{bCn\_I} - m\left(u_{bCn\_I} - u_{bCn\_K}\right)\right] \quad (29)$$

$$\lambda_{on\_3} = i_{bLn} - i_{bLn\_T} + \frac{U_{inn}}{i_{bOn}}\left(u_{bCn} - u_{bCn\_T}\right) \quad (30)$$

In an actual design, a hysteresis width around U_{bCn_I}, which affects the voltage ripple, needs to be considered. The range of the parameter m is $0 \le m \le 1$. The smaller m, the smaller the voltage deviation, and the longer the recovery time. When m=1, the path coincides with the natural trajectory. The voltage deviation is the largest and the recovery time is the shortest.

IV. The Performance-Optimal Synthetic Controls

From the preceding deductions, the Boost converter cannot simultaneously obtain the minimum voltage deviation and the shortest recovery time. However, the minimum voltage deviation trajectory is required in some cases. In most cases, considering the requirements of the converter, a reasonable tradeoff between the shortest recovery time and the minimum voltage fluctuation is required. Through an analysis, it is determined that the output voltage deviation is more obvious than the inductor current fluctuation when the load suddenly increases. When the load suddenly decreases, the inductor current fluctuation is more obvious than the output voltage deviation.

A. The Relationship between the Recovery Time and the Voltage Deviation

This section discusses the variation of the recovery time and the voltage deviation with the control parameter m in (29).

If the switch is turned off after Point I when the load suddenly increases, there are two possible paths, HMNT and HKQT, which are shown in Fig. 13. The principle of selecting a path is to guarantee the demand voltage deviation and to shorten the recovery time as much as possible. Therefore, the

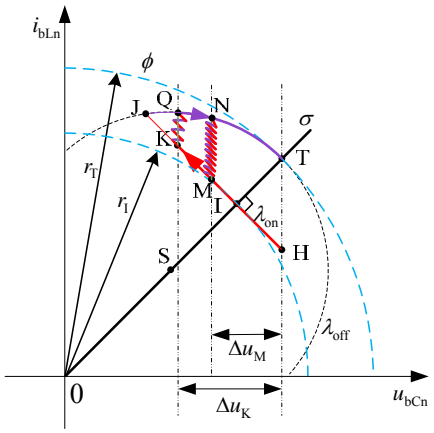

Fig. 13. Two paths in boost converters.

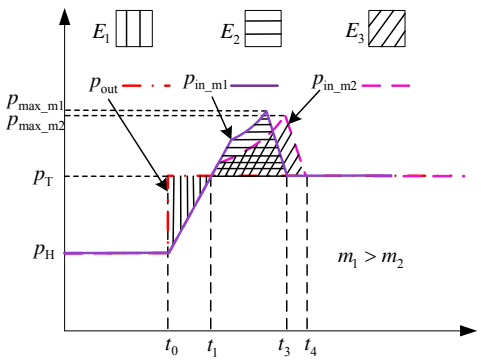

Fig. 14. The relationship between energy and time.

path needs to follow the on-state and off-state natural trajectories as far as possible. In Fig. 13, it can be seen that the recovery time of Path HMNT is higher than the recovery time of Path HKQT due to the geometric relationship and $\Delta u_K > \Delta u_M$.

The relationship between the voltage deviation and the parameter m in load suddenly increase is as follows:

$$\Delta u_{bc} = u_{bCn\_T} - u_{bCn\_M} = u_{bCn\_T} - \left[u_{bCn\_I} - m\left(u_{bCn\_I} - u_{bCn\_K}\right)\right] \tag{31}$$

In the view of the storage energy change in the converters, the slopes of the increased and decreased input power, which are proportional to the inductor current, are constant in terms of different control parameters m, as shown in Fig. 14. The different regions at the input and output powers can be approximated as two triangles.

The energy storage change of the inductance current is:

$$\Delta E_{bL} = \frac{1}{2}L_b {i_{bL\_T}}^2 - \frac{1}{2}L_b {i_{bL\_H}}^2 = E_{2\_k1} - E_1 = E_{2\_k2} - E_1 \tag{32}$$

The time when the inductor current rises to the target current is from t_0 to t_1:

$$t_{01} = \frac{L_b\left(i_{bL\_T} - i_{bL\_H}\right)}{U_{in}} \tag{33}$$

Then:

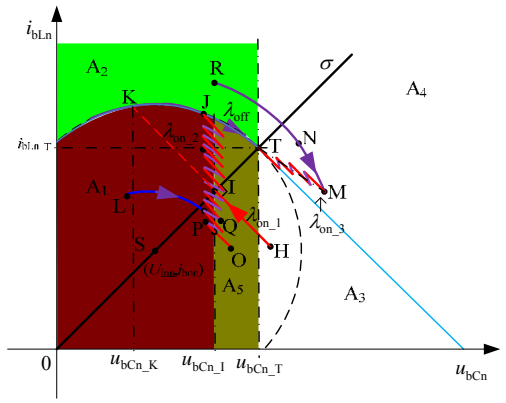

Fig. 15. The performance-optimal synthetic control path.

$$E_1 = \frac{\left(p_T - p_U\right)}{2}t_{01} = \frac{\left(U_{in}i_{bL\_T} - U_{in}i_{bL\_H}\right)}{2}t_{01} = \frac{L_b\left(i_{bL\_T} - i_{bL\_H}\right)^2}{2} \tag{34}$$

The compensation energy is:

$$E_{2\_m1} = E_{2\_m2} = E_1 + \Delta E_{bL} = \frac{L_b\left(i_{bL\_T} - i_{bL\_H}\right)^2}{2} + \frac{L_b\left({i_{bL\_T}}^2 - {i_{bL\_H}}^2\right)}{2} \tag{35}$$

The compensation time in m is:

$$t_{1m} = \frac{2E_{2\_m}}{p_{max\_m} - p_T} = \frac{2E_{2\_m}}{U_{in}\left(i_{bL\_M} - i_{bL\_T}\right)} \tag{36}$$

The totally recovery time is:

$$t_r = t_{01} + t_{1k} = \frac{L_b\left(i_{bL\_T} - i_{bL\_H}\right)}{U_{in}} + \frac{2E_{2\_k}}{U_{in}\left(i_{bL\_M} - i_{bL\_T}\right)} \tag{37}$$

It is shown that the bigger the value of m, the bigger the input power, and the bigger the value of i_{bL_M}. In addition, the shorter the recovery time, the shorter the total recovery time.

B. The Relationship between the Recovery Time and the Current Fluctuation

When the load suddenly decreases, the inductor current fluctuation is more obvious. On the basis of the minimum voltage deviation trajectory, the slope of the on-state natural trajectory in the A_4 region should be enlarged to reduce the current fluctuation, as in segment MT in Fig. 15.

The SS equation is:

$$\lambda_{on\_3} = i_{bLn} - i_{bLn\_T} + h\frac{U_{inn}}{i_{bOn}}\left(u_{bCn} - u_{bCn\_T}\right) \tag{38}$$

The range of h is $0<h\leq 1$. The bigger the value of h, the bigger the current fluctuations, and the shorter the recovery time. When h=1, the path coincides with the natural trajectory, and the recovery time is the shortest.

It can be seen that the proposed SS is based on a combination of the natural trajectories. In addition, according to the boundary control of the stability criterion [17], [19], both

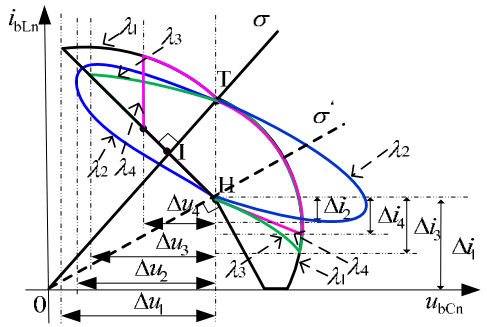

(a) Sketch.

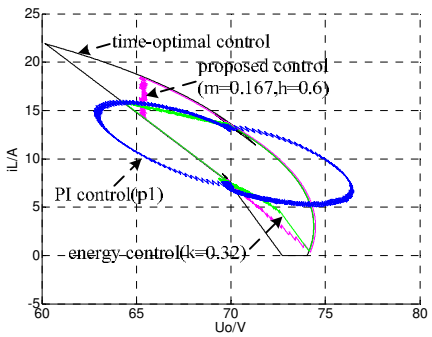

(b) Simulation.

Fig. 16. Four control trajectory.

of the sides in the natural SS are a reflection or a refraction. This means that the natural SS is located in stable areas, and that the control law is as stable as the other laws mentioned in the literature [20], [33].

V. The Comparison of Control Effect in Four Control Trajectories

The phase plane diagram and the simulation phase plane are described in Fig. 16, where λ_1 is the minimum time trajectory, λ_2 is the PI control trajectory, λ_3 is the energy control trajectory used in [33], and λ_4 is the performance-optimal synthetic control trajectory proposed in this paper.

When the load suddenly increases, the operating point changes from Point H to Point T. λ_1 is composed of one on-state natural trajectory and one off-state natural trajectory. λ_2 is composed of multiple on-state natural trajectories and multiple off-state natural trajectories. λ_3 is composed of one on-state natural trajectory and one assembled trajectory. λ_4 is composed of one on-state nature trajectory, one off-state nature trajectory, and one assembled trajectory. In accordance with the indicated control parameter in Fig. 16(b), the voltage deviation relation is $\Delta u_1 > \Delta u_2 > \Delta u_3 > \Delta u_4$. Following the principles that the assembled path is longer and the recovery time is higher in the same voltage deviation, the assembled path in λ_4 is less than the path in λ_3, and the assembled path in λ_2 is longer than the path in λ_3 or λ_4. Therefore, the recovery time relation is $t_{r1} < t_{r4} < t_{r3} < t_{r2}$.

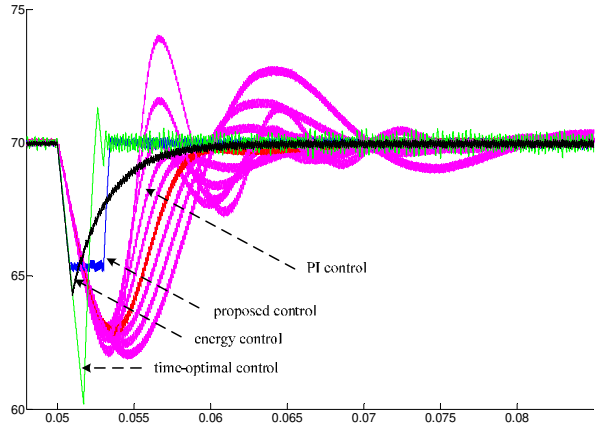

Fig. 17. The output voltage comparison of all kinds of PI parameters and others three control methods.

When the load suddenly decreases, the operating point changes from Point T to Point H. λ_1 is composed of one time on-state natural trajectory, one time off-state natural trajectory, and one possible path where the current is zero (DCM). λ_2 is composed of multiple on-state natural trajectories and multiple off-state natural trajectories. λ_3 is composed of one time off-state natural trajectory and one time assembled trajectory. λ_4 is composed of one time off-state natural trajectory and one time assembled trajectory. In accordance with the indicated control parameter in Fig. 16(b), the current fluctuation relation is $\Delta i_1 > \Delta i_3 > \Delta i_4 > \Delta i_2$. In the same current fluctuation, the assembled path in λ_4 is less than the path in λ_3; and the assembled path in λ_2 is longer than the path in λ_3 or λ_4. Therefore, the recovery time relation is $t_{r1} < t_{r4} < t_{r3} < t_{r2}$.

In these four control methods, only the switching frequency of the PI control is fixed. In the test setup, the switching frequency of the PI control is 10 kHz. In comparison, the switching frequencies of the other control methods are variable. The equivalent switching frequency of the time-optimal control method is about 16.67 kHz, and so is the proposed control method. The equivalent switching frequency of the energy control method is about 16.25 kHz.

The PI control, as a kind of frequency domain method, cannot get the theoretical optimum value unlike the time-optimal control method and the proposed control method.

Fig. 17 shows a comparison of the PI control with all kinds of P and I parameters and the other three trajectory control methods. It can be that that no matter how the PI parameters change, its performance cannot approach the theoretical value when compared with the time-optimal control or the proposed control.

A. The Simulation Comparison of the Control Effects in the Four Control Trajectories

The simulation circuit uses the parameters listed in Table I. To make the differences between the four control methods more significant, the circuit parameters are deliberately designed like this. When the load suddenly decreases from 20

TABLE I
PARAMETERS OF THE CIRCUIT

Input voltage U_{in}	30 V
Output voltage u_o	70 V
Inductance L_b	3.35 mH
Capacitance C_b	950 uF
Sampling Frequency f_s	40 kHz

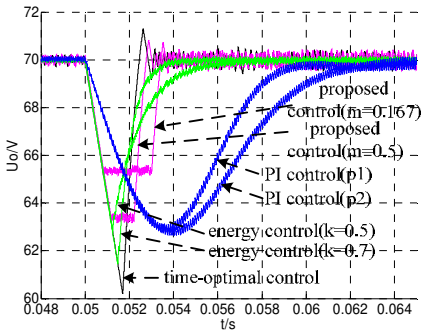

(a)

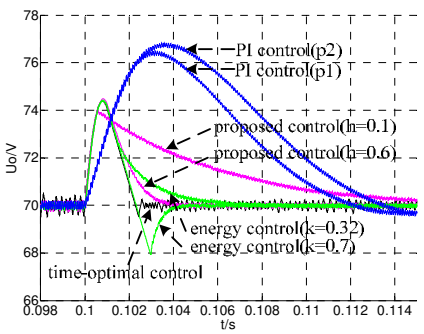

(b)

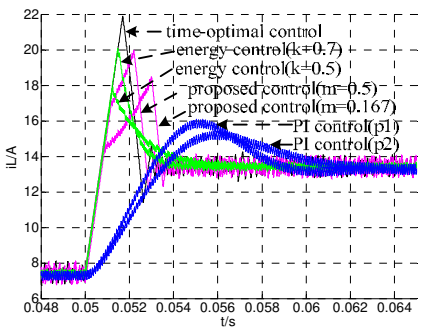

(c)

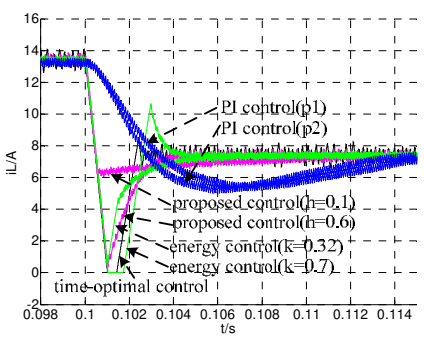

(d)

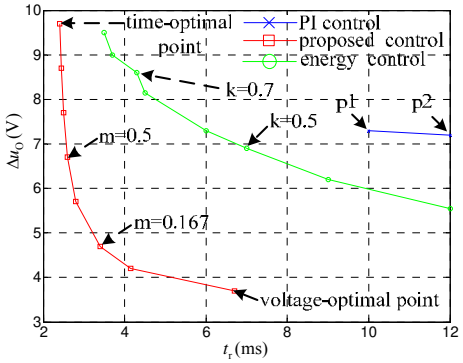

(e)

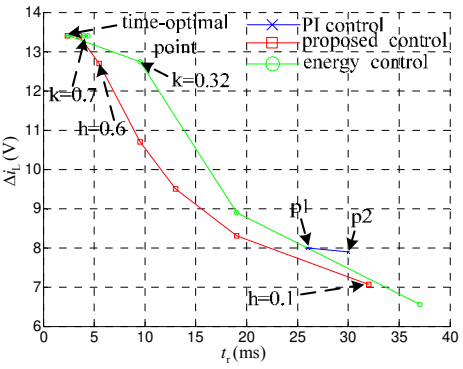

(f)

Fig. 18. Comparisons of four control trajectories in different parameters. (a) Capacitor voltage waveforms when load suddenly increases. (b) Capacitor voltage waveforms when load suddenly decreases. (c) Inductor current waveforms when load suddenly increases. (d) Inductor current waveforms when load suddenly decreases. (e) The relationship between voltage deviation and recovery time when load suddenly increases. (f) The relationship between current fluctuation and recovery time when load suddenly decreases.

Ω to 10 Ω and then suddenly increases to 20 Ω for a while, the simulation waves in the four control trajectories are shown in Fig. 18. The three trajectories use several sets of parameters to acquire the relationship between the voltage deviation and the recovery time; and the relationship between the current fluctuation and the recovery time. The simulation results indicates that the proposed method can achieve the optimal effect in the four methods.

B. The Experiment Comparison of the Control Effect in the Four Control Trajectories

In order to confirm the correctness of the theoretical analysis and to verify the validity of the proposed synthetic control, a 500 W Boost converter prototype is established. A digital signal processor (DSP) TMS320F28335 which samples at 40 kHz is utilized for the experiment. The parameters in the experimental circuit are the same as those listed in Table I.

1) Load Suddenly Increases

The experimental waveforms with the four trajectories in

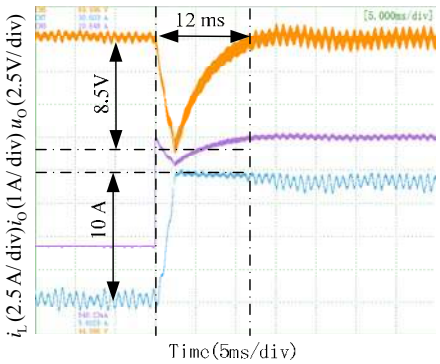

(a)

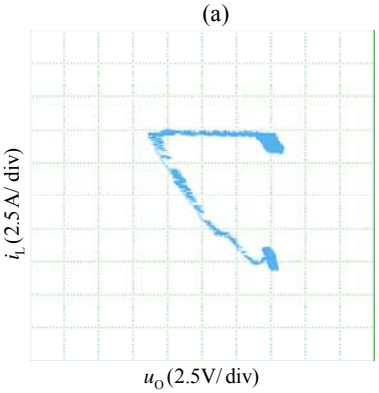

(b)

Fig. 19. Experimental results of PI control. (a) Capacitor voltage, output current and inductor current. (b) Phase plane.

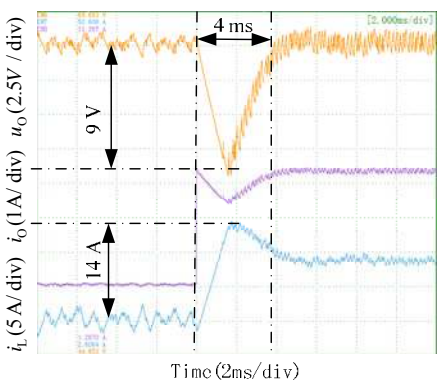

(a)

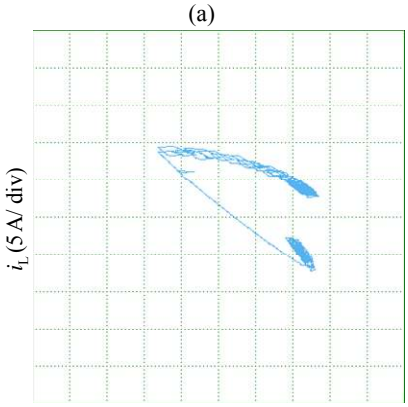

(b)

Fig. 20. Experimental results of time-optimal control. (a) Output voltage, output current and inductor current. (b) Phase plane.

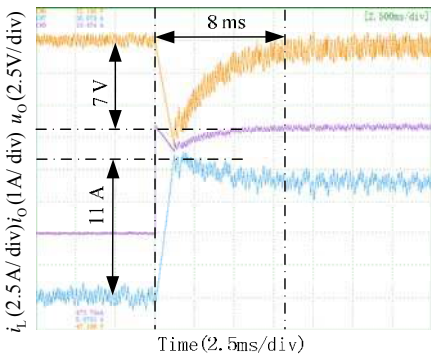

(a)

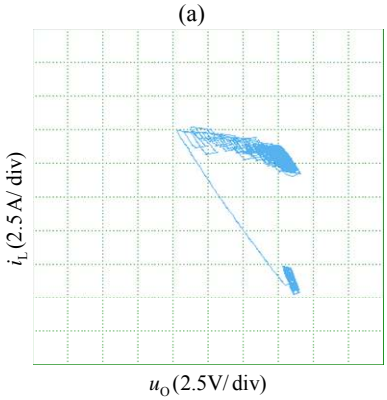

(b)

Fig. 21. Experimental results of energy control (k=0.38). (a) Output voltage, output current and inductor current. (b) Phase plane.

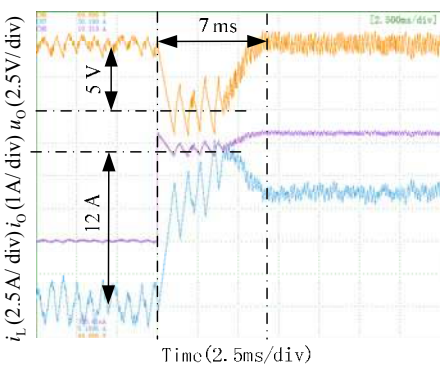

(a)

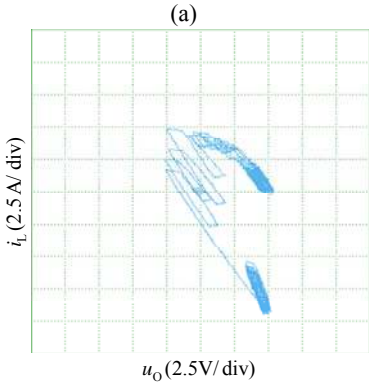

(b)

Fig. 22. Experimental results of proposed control (m=0.38). (a) Output voltage, output current and inductor current. (b) Phase plane.

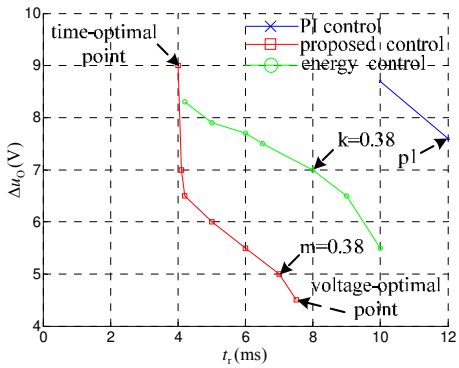

Fig. 23. The relationship between voltage deviation and recovery time in four control methods

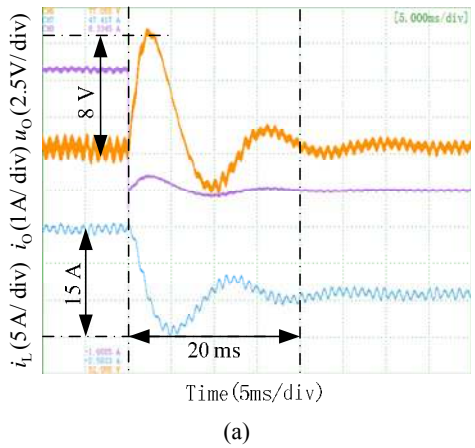

(a)

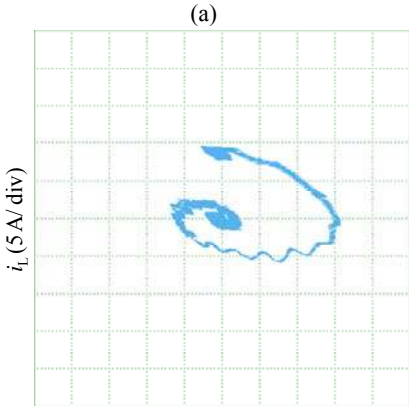

(b)

Fig. 24. Experimental results of PI control. (a) Output voltage, output current and inductor current. (b) Phase plane.

different parameters are shown in Fig. 19 to Fig. 22 when the load changes from 20Ω to 10Ω. An experimental comparison of the PI control, the time-optimal control, the energy control and the proposed control is shown in Fig. 23. This is in agreement with the simulation in Fig. 18(e) and the theoretical analysis. Some differences, such as the voltage ripple in Fig. 21(a), are caused by limited sampling and the control frequency in the actual circuit, and ESR in the capacitor (R_C=0.09Ω).

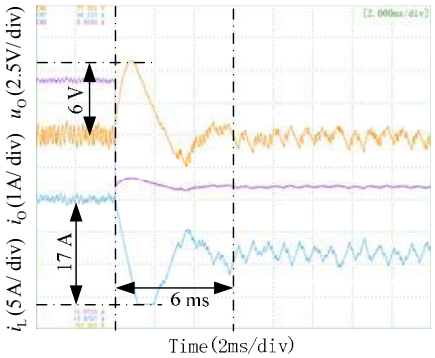

(a)

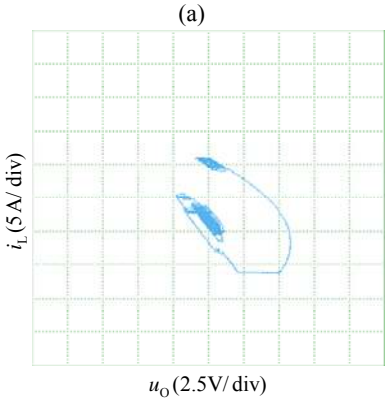

(b)

Fig. 25. Experimental results of time-optimal control. (a) Output voltage, output current and inductor current. (b) Phase plane.

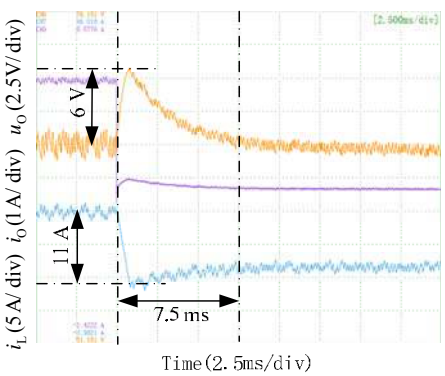

(a)

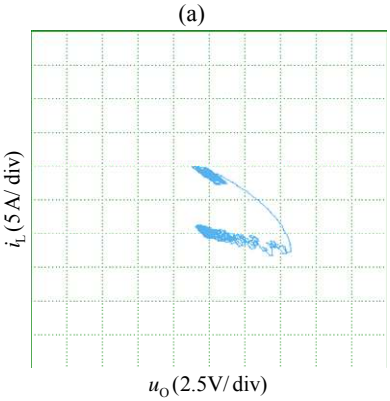

(b)

Fig. 26. Experimental results of energy control (k=0.18). (a) Output voltage, output current and inductor current. (b) Phase plane.

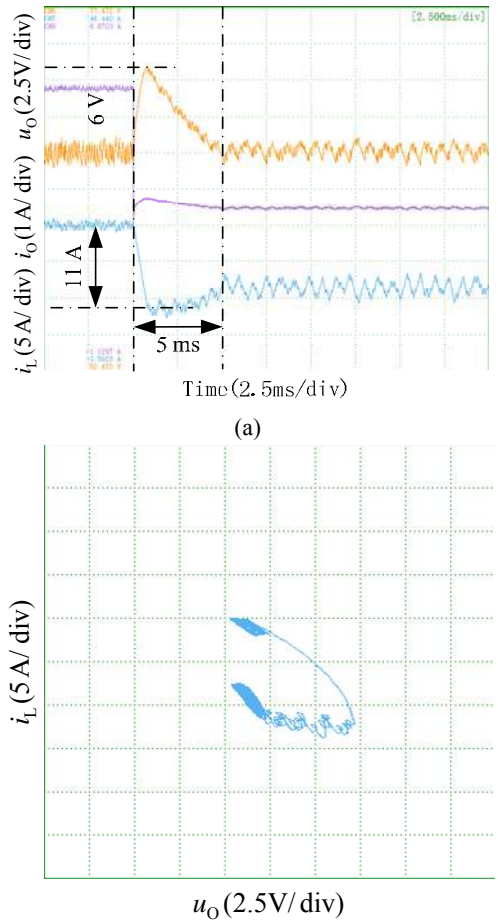

Fig. 27. Experimental results of proposed control (h=0.1). (a) Output voltage, output current and inductor current. (b) Phase plane.

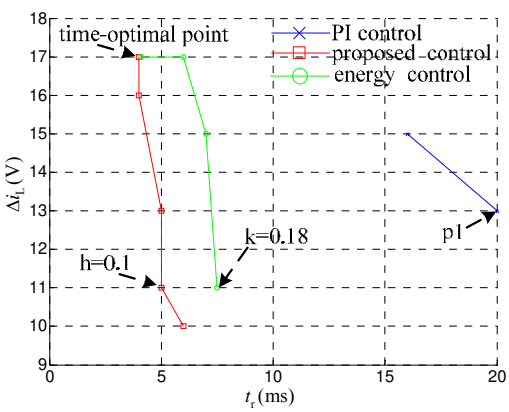

Fig. 28. The relationship between current fluctuation and recovery time in four control methods.

2) Load Suddenly Decreases

The experimental waveforms with the four trajectories in different parameters are shown in Fig. 24 to Fig. 27 when load changes from 10Ω to 20Ω. An experimental comparison of the PI control, the time-optimal control, the energy control and the proposed control is shown in Fig. 28. This is in agreement with the simulation in Fig. 18(f) and the theoretical analysis.

Although the experimental results are not as good as the simulation results due to various non-ideal factors, it can be seen that the synthetic optimized control has much better transient performance than the previous control methods.

VI. Conclusion

For the transient performance of a Boost converter, on the basis of the minimum recovery time trajectory, this paper proposes the minimum voltage deviation trajectory combined with the converter storage energy change law, and proposes a transient performance-optimal synthetic control trajectory in the boundary control method. The experimental results obtained from a 500-W prototype are in agreement with the theoretical analysis. The results also show that the proposed method can achieve a better transient performance than the other control methods.

Acknowledgment

Supported by National Natural Science Foundation of China (51577100, 51490683) and by the Program of State Key Laboratory of Power System in Tsinghua University (SKLD15Z01). The authors would like to thank the State Grid Corporation of China for the support of the project titled Research on the Energy Router in the Distribution Network for the Energy Internet.

References

[1] C. K. Tse and M. D. Bernardo, "Complex behavior in switching power converters," *Proceedings of the IEEE*, Vol. 90, No. 5, pp. 768-781, May 2002.

[2] W. Jiang and F. Yuan "Study of nonlinear phenomena in power electronic circuit," in *International Conference on Energy and Environment Technology(ICEET)*, Vol. 2, pp. 309-312, Oct. 2009.

[3] Y. Qiu, M. Xu, K. Yao, J. Sun, and F. C. Lee, "The multi-frequency small-signal model for buck and multiphase interleaving buck converters," in *20th Annual IEEE Applied Power Electronics Conference and Exposition(APEC)*, Vol. 1, pp. 392-398, Mar. 2005.

[4] J. M. Galvez, M. Ordonez, and M. Anun, "Normalized geometrical analysis: unified theory and derivation of natural trajectories for basic dc-dc topologies," in *IEEE 14th Workshop on Control and Modeling for Power Electronics(COMPEL)*, pp. 1-5, Jun. 2013.

[5] L. E. Armin and M. Salimi, "Passivity-based control of the DC-DC buck converters in high-power applications," *Journal of Artificial Intelligence in Electrical Engineering*, Vol. 2, No. 8, pp. 48-58, Mar. 2014.

[6] Y. I. Son and I. H. Kim, "Complementary PID controller to passivity-based nonlinear control of boost converters with inductor resistance," *IEEE Trans. Control Syst. Technol.*, Vol. 20, No. 3, pp. 826-834, May 2012.

[7] M. Salimi, J. Soltani, A. Zakipour, and N. R. Abjadi, "Hyper-plane sliding mode control of the DC-DC buck/boost converter in continuous and discontinuous

conduction modes of operation," *IET Power Electronics*, Vol. 8, No. 8, pp. 1473-1482, Feb. 2015.

[8] A. Agarwal, K. Deekshitha, S. Singh, and D. Fulwani, "Sliding mode control of a bidirectional DC/DC converter with constant power load," in *IEEE 1st International Conference on DC Microgrids(ICDCM)*, pp. 287-292, Jun. 2015.

[9] L. Rui, D. Maksimovic, and R. Leyva, "State-machine realization of second-order sliding-mode control for synchronous buck DC-DC converters," in *IEEE Energy Conversion Congress and Exposition(ECCE)*, pp. 125-132, Sep. 2013.

[10] A. J. Mehta and B. B. Naik, "Adaptive sliding mode controller with modified sliding function for DC-DC boost converter," in *Conference on Power Electronics, Drives and Energy Systems(PEDES)*, pp. 1-5, 2014.

[11] K. M. Smedley and S. Cuk, "One-cycle control of switching converters," *IEEE Trans. Power Electron.*, Vol. 10, No. 6, pp. 625-633, Nov. 1995.

[12] K. Subramanian, V. K. S. Kumar, E. M. Saravanan, and E. Dinesh, "Improved one cycle control of DC-DC buck converter," in *International Conference on Advanced Communication Control and Computing Technologies (ICACCCT)*, pp. 219-223, May 2014.

[13] I. Kondratiev, E. Santi, R. Dougal, and G. Veselov, "Synergetic control for DC-DC buck converters with constant power load," in *IEEE 35th Annual Power Electronics Specialists Conference(PESC)*, Vol. 5, pp. 3758-3764, Jun. 2004.

[14] I. Kondratiev, E. Santi, and R. Dougal, "Robust nonlinear synergetic control for m-parallel-connected DC-DC boost converters," in *IEEE Power Electronics Specialists Conference*, pp. 2222-2228, Jun. 2008.

[15] R. Stadlmayr and K. Schlacher, "An energy-based control strategy for dc/dc power converters," in *European Control Conference(ECC)*, pp. 3967-3972, Aug. 2009.

[16] X. Mao, S. Falcones, and R. Ayyanar, "Energy-based control design for a solid state transformer," in *IEEE Power and Energy Society General Meeting*, pp. 1-7. Jul. 2010.

[17] R. Munzert and P. T. Krein, "Issues in boundary control [of power convertors]," in *27th Annial IEEE Power Electronics Specialists Conference(PESC)*, Vol. 1, pp. 810-816, Jun. 1996.

[18] I. G. Zurbriggen, M. Ordonez, and M. Anun, "Average natural trajectories (ANTs) for buck converters: centric-based control," in *28th Annual IEEE Applied Power Electronics Conference and Exposition(APEC)*, pp. 1346-1351, Mar. 2013.

[19] C. N. Onwuchekwa and A. Kwasinski, "Analysis of boundary control for buck converters with instantaneous constant-power loads," *IEEE Trans. Power Electron.*, Vol. 25, No. 8, pp. 2018-2032, Aug. 2010.

[20] J. M. Galvez, M. Ordonez, F. Luchino, and J. E. Quaicoe, "Improvements in boundary control of boost converters using the natural switching surface," *IEEE Trans. Power Electron.*, Vol. 26, No.11, pp. 3367-3376, Nov. 2011.

[21] P. K. W. Chan, H. S. H. Chung and S. Y. Hui, "A generalized theory of boundary control for a single-phase multilevel inverter using second-order switching surface," *IEEE Trans. Power Electron.*, Vol. 24, No. 10, pp. 2298-2313, Oct. 2009.

[22] J. Y. Chiu, K. K. Leung, and H. S. Chung, "High-order switching surface in boundary control of inverters," *IEEE Trans. Power Electron.*, Vol. 22, No. 5, pp. 1753-1765, Sep. 2007.

[23] J. Ge, Z. Zhao, L. Yuan, T. Lu, and F. He, "Direct power control based on natural switching surface for three-phase PWM rectifiers," *IEEE Trans. Power Electron.*, Vol. 30, No. 6, pp. 2918-2922, Jun. 2015.

[24] J. M. Galvez and M. Ordonez, "High performance boundary control of boost-derived PFCs: natural switching surface derivation and properties," *IEEE Trans. Power Electron.*, Vol. 27, No. 8, pp. 3807-3816, Aug. 2012.

[25] Y. Zhang, X. Ge, and X. Wu, "Analysis and design of a ZVS boost/buck-boost dual mode PFC converter with universal input and wide output voltages," in *1st International Future Energy Electronics Conference (IFEEC)*, pp. 36-41, Nov. 2013.

[26] G. G. Oggier, M. Ordonez, J. M. Galvez, and F. Luchino, "Fast transient boundary control and steady-state operation of the dual active bridge converter using the natural switching surface," *IEEE Trans. Power Electron.*, Vol. 29, No. 2, pp. 946-957, Feb. 2014.

[27] C. N. Onwuchekwa and A. Kwasinski, "Analysis of boundary control for boost and buck-boost converters in distributed power architectures with constant-power loads," in *26th Annual IEEE Applied Power Electronics Conference and Exposition(APEC)*, pp. 1816-1823, Mar. 2011.

[28] W. Yan, C. N. Ho, H. S. Chung, and K. T. K. Au, "Fixed-frequency boundary control of buck converter with second-order switching surface," *IEEE Trans. Power Electron.*, Vol. 24, No. 9, pp. 2193-2201, Sep. 2009.

[29] J. Y. Chiu, K. K. Leung, and H. S. Chung, "High-order switching surface in boundary control of inverters," *IEEE Trans. Power Electron.*, Vol. 22, No. 5, pp. 1753-1765, Sep. 2007.

[30] M. Ordonez, M. T. Iqbal, and J. E. Quaicoe, "Selection of a curved switching surface for buck converters," *IEEE Trans. Power Electron.*, Vol. 21, No. 4, pp. 1148-1153, Jul. 2006.

[31] J. M. Galvez, M. Ordonez, F. Luchino, and J. E. Quaicoe, "Improvements in boundary control of boost converters using the natural switching surface," *IEEE Trans. Power Electronics*, Vol. 26, No. 11, pp. 3367-3376, Nov. 2011.

[32] M. Ordonez, J. E. Quaicoe, and M. T. Iqbal, "Advanced boundary control of inverters using the natural switching surface: normalized geometrical derivation," *IEEE Trans. Power Electron.*, Vol. 23, No. 6, pp. 2915-2930, Nov. 2008.

[33] J. Ge, L. Yuan, Z. Zhao, T. Lu, F. He, and G. Feng, "Tradeoff between the output voltage deviation and recovery time of boost converters," *Journal of Power Electronics*, Vol. 15, No. 2, pp. 338-345, Mar. 2015.

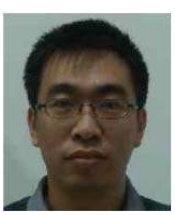

Gaohui Feng received his B.S. and M.S. degrees from the Mechanical Engineering College, Shijiazhuang, China, in 2002 and 2005, respectively. He is presently working towards his Ph.D. degree at the State Key Laboratory for the Control and Simulation of Power Systems and Generation Equipment, Department of Electrical Engineering, Tsinghua University, Beijing, China. His current research interests include high-voltage and high-power converter designs, and digital control techniques.

Liqiang Yuan received his B.S. and Ph.D. degrees from Tsinghua University, Beijing, China, in 1999 and 2004, respectively. He became an Assistant Professor, in 2004, and an Associate Professor, in 2008, in the Department of Electrical Engineering, Tsinghua University. His current research interests include the application techniques of semiconductor devices, photovoltaic systems, and high power high voltage converters.

Zhengming Zhao received his B.S. and M.S. degrees in Electrical Engineering from Hunan University, Changsha, China, in 1982 and 1985, respectively. He received his Ph.D. degree from Tsinghua University, Beijing, China, in 1991, and then worked in the Department of Electrical Engineering, Tsinghua University. From 1994 to 1996, he was a Postdoctoral Fellow at Ohio State University, Columbus, OH, USA. The following year, he worked as a Visiting Scholar at the University of California, Irvine, CA, USA. He is presently a Professor in Department of Electrical Engineering, Tsinghua University. He is also the Deputy Director of the State Key Lab of Power Systems, the Vice President of the Beijing Power Electronic Society, the Chairman of the IEEE PELS Beijing Chapter, and an IET Fellow. Dr. Zhao′s current research interests include high power conversions, power electronics, motor control, and solar energy applications.

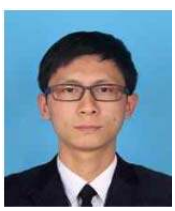

Junjie Ge was born in Hubei, China. He received his B.S. degree in Hydroelectric Power Engineering from the Huazhong University of Science and Technology, Wuhan, China, in 2010. He received his Ph.D. degree in Electrical Engineering from Tsinghua University, Beijing, China, in 2015. He is presently working as a Scientist in the ABB Corporate Research Center, Beijing, China. His current research interests include power electronics converters and DC microgrids.

Xiuxi Ye received his B.S. and M.S. degrees from the Mechanical Engineering College, Shijiazhuang, China, in 2005 and 2008, respectively. He is presently working towards his Ph.D. degree at the State Key Laboratory for the Control and Simulation of Power System and Generation Equipment, Department of Electrical Engineering, Tsinghua University, Beijing, China. His current research interests include power electronic converters, solid-state transformers, and digital control techniques.

Ting Lu received his B.S. and Ph.D. degrees in Electrical Engineering from Tsinghua University, Beijing, China, in 2005 and 2010, respectively. From 2010 to 2012, he was a Postdoctoral Fellow in the Department of Electrical Engineering, Tsinghua University. Since 2012, he has been an Assistant Professor in the Department of Electrical Engineering, Tsinghua University. His current research interests include the application techniques of high power semiconductor devices, and the control strategies of high power high voltage converters.